

Fully passive quantum secure direct communication

Jia-Wei Ying,¹ Qi Zhang,² Shi-Pu Gu,¹ Xing-Fu Wang,² Lan Zhou,^{2*} and Yu-Bo Sheng^{1†}
¹*College of Electronic and Optical Engineering and College of Flexible Electronics (Future Technology),
Nanjing University of Posts and Telecommunications,
Nanjing, 210023, China*
²*College of Science,
Nanjing University of Posts and Telecommunications,
Nanjing, 210023, China*

(Dated: February 19, 2025)

In practical quantum communication, imperfect devices may introduce side channels, creating opportunities for eavesdroppers. Especially on the source side, the side channels created by active modulation are vulnerable to trojan horse attacks. Utilizing passive sources presents an effective solution to this issue. This paper proposes a fully passive quantum secure direct communication (QSDC) protocol. By passively modulating both the quantum state and the intensity of the decoy state, we can effectively eliminate the side-channel risks associated with the source modulators, thereby enhancing the security of practical QSDC. We optimize the intensities of the fully passive QSDC protocol to identify the optimal pulse performance of different post-selection intervals under various channel attenuation conditions. The numerical simulation results indicate that the secrecy message capacity of fully passive QSDC can reach $1.34 * 10^{-3}$ ($3.10 * 10^{-4}$) bit/pulse at 5 (10) km, approximately 78.0% (75.7%) of that of actively modulated QSDC. In addition, we consider the resource consumption and detection efficiency, optimizing the size of the post-selection intervals to obtain the optimal secrecy message transmission rate corresponding to each channel attenuation. Its maximum communication range is about 17.75 km. At communication distances of 5 (10) km, the maximum secrecy message transmission rate of a source with a pulse frequency of 10^6 Hz is 10.268 (1.351) bit/sec. Our work significantly contributes to enhancing the security of practical QSDC systems.

I. INTRODUCTION

Quantum communication has garnered significant attention due to its unconditional security. Quantum secure direct communication (QSDC) is a branch of quantum communication, which can directly transmit message. The first QSDC protocol was proposed in 2002 [1], and subsequent research has yielded numerous theoretical [2–11] and experimental [12–20] results. As theoretical and experimental understandings deepen, the practical security of quantum communication has become an area of increasing focus [21–26]. Quantum communication is theoretically unconditionally secure, while imperfections in actual experimental equipment can introduce side channels that may be exploited by eavesdroppers [27–31]. The sources and detectors are particularly critical in this context.

In 2012, the measurement-device-independent (MDI) quantum key distribution (QKD) protocol was proposed [32], which can eliminate all side channels on the detector side, significantly enhancing the security of QKD [33–36]. In the field of QSDC, MDI was applied to QSDC in 2020 and successfully eliminated the side channels associated with QSDC detectors [37, 38]. Subsequently, there are many studies on MDI-QSDC [39–42]. While these efforts

focused on defending against side channels of the detectors, addressing vulnerabilities at the source is equally important.

An effective countermeasure for the imperfect source is the device-independent (DI) protocol [43–49], which can resist all attacks targeting both detectors and sources. DI QKD was proposed in 2007 [43] and experimentally demonstrated in 2022 [50–52]. However, DI is very sensitive to loss, it needs state-of-the-art devices, and the communication distance and key rate are still limited [53].

Another measure to improve the security of sources is to use passive sources. In quantum communication, we usually need to perform some modulation operations on the source. This is especially true in the decoy state method [18, 26, 54, 55], where we have to modulate both the light intensity and the quantum state. These modulation processes, both intensity and state, will introduce side channels, creating opportunities for eavesdropper [22]. One notable threat is the trojan horse attack [56–59]. The eavesdropper injects a pulse into the light source, and the trojan horse pulse is modulated with the signal pulse and reflected through the device into the channel. Eve can analyze reflected pulses to obtain information. The advantage of a passive source is that it eliminates the need for active modulation of the source, thereby removing the side channels associated with the source modulator. This setup can effectively resist side-channel attacks targeting the modulator. Passive decoy states [60–66] and passive coding [67–71] have been widely applied in quantum communication. Re-

* zhou@njupt.edu.cn

† shengyb@njupt.edu.cn

cently, the fully passive QKD has been proposed [72], which combines passive decoy states and passive coding. It employs four phase-random coherent pulses to generate a random quantum state with random intensity through beam splitter(BS) interference and polarization beam splitter(PBS) combination. By post-selecting the output photon pulses, the desired state can be obtained.

Passive sources have been incorporated into many quantum communication protocols[73–78] and have been experimentally validated[79, 80]. Inspired by the previous work [72–80], we proposed the fully passive QSDC. By integrating fully passive source with QSDC, we can effectively resist the side channel attack against QSDC source, so as to improve the security of practical QSDC protocol. This paper mainly makes the following contributions: (1) Based on the fully passive source, we establish a QSDC system model, and give the formula of its secrecy message capacity, as well as the complete analysis process. (2) We optimize the intensities of fully passive QSDC, and give the optimal input light intensity to maximize the secrecy message capacity of each channel attenuation. It is compared with the optimal case of the actively modulated QSDC. Meanwhile, considering the resource consumption and detection efficiency, we optimize the size of the post-selection intervals, and obtain the optimal secrecy message transmission rate corresponding to each channel attenuation. The structure of the paper is as follows. In Sec. II, we introduce the fully passive QSDC protocol. In Sec. III, we give the system model of the fully passive QSDC and analyze the secrecy message capacity based on decoy-state method. In Sec. IV, we conduct numerical simulation and parameter optimization. In Sec. V, we give a conclusion.

II. THE FULLY PASSIVE QSDC PROTOCOL

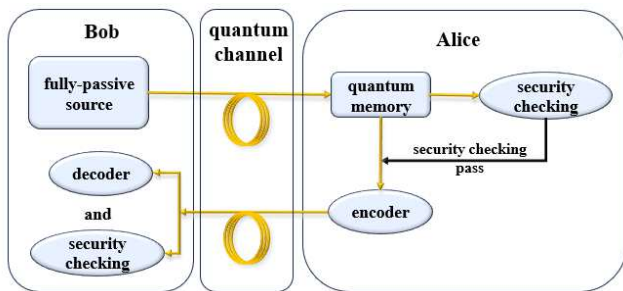


FIG. 1. The structure of the fully passive QSDC protocol.

In this section, we explain our fully passive QSDC protocol. As shown in Fig. 1, there are two participants, the message sender Alice and the message receiver Bob. The fully passive QSDC protocol can be described as follows.

Step 1: Initial state preparation. The message receiver Bob generates a series of weak coherent pulses through

a fully passive source(details in section III.A). The intensities of these pulses are random, and the photons in them are in the quantum state $a^\dagger(\theta, \phi)$ (details in section III.A). Then Bob filters the desired quantum states and pulse intensities through the post-selection module and sends them to Alice.

Step 2: First round of security checking. Alice receives these pulses and stores them in quantum memory. Then randomly select a part of the pulses to perform the first round of security checking, which is similar to QKD. Through security checking, Alice can estimate the error rate E1. If E1 is below the tolerate threshold E^{BA} (details in section III.C), the communication continues. Otherwise, the parties have to discard the communication.

Step 3: Encoding. After the security checking is passed, Alice takes out the remaining photons in the quantum memory, selects some of them for random encoding for the second round of security checking, and encodes the rest for information with the operations I and Y , where $I = |H\rangle\langle H| + |V\rangle\langle V|$ and $Y = i\sigma_y = |H\rangle\langle V| - |V\rangle\langle H|$. I and Y represent the classical messages 0 and 1, respectively. Then, send the pulses to Bob.

Step 4: Second round of security checking. Bob selects the X or Z basis to decode the received pulse based on the initial pulse information. Then Alice announces the position of the randomly encoding pulses and the randomly encoded information, and Bob estimates the error rate E2 based on the measurement results of the corresponding position. If E2 is below the tolerate threshold E^{BAB} (details in section III.C), the communication continues. Otherwise, the parties have to discard the communication.

Step 5: Decoding. Bob deduces Alice's encoded information from the measurements of the remaining photons and his own initial states.

III. SYSTEM MODEL

A. The fully passive source

In the protocol, we use a symmetric fully passive source [73], whose structure is shown in the Fig. 2. Among them, the initial four coherent pulses are as follows:

$$\begin{aligned} |\mu_1\rangle &= |\sqrt{v}e^{i\alpha}\rangle_R, |\mu_2\rangle = |\sqrt{v}e^{i\beta}\rangle_R, \\ |\mu_3\rangle &= |\sqrt{v}e^{i\gamma}\rangle_L, |\mu_4\rangle = |\sqrt{v}e^{i\delta}\rangle_L, \end{aligned} \quad (1)$$

where α, β, γ , and δ are random phases of the four pulses, and the pulses have the same intensity v . The subscripts R and L represent the quantum state of the particles in the pulse. R corresponds to the quantum state $|R\rangle = \frac{1}{\sqrt{2}}(|H\rangle + i|V\rangle)$ and L corresponds to the quantum state $|L\rangle = \frac{1}{\sqrt{2}}(|H\rangle - i|V\rangle)$. Here, H and V represent the horizontal and vertical polarization of the photons.

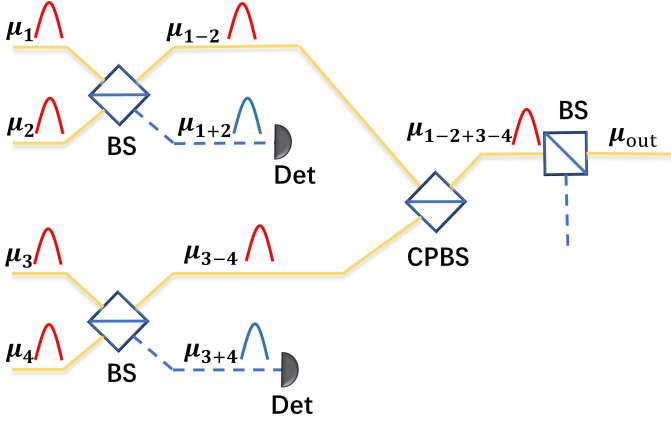


FIG. 2. The structure of the symmetric fully passive source, which is similar to that in [73]. BS: beam splitter; CPBS: circular polarization beam splitter; Det: detector.

Firstly, input pulses $|\mu_1\rangle$ and $|\mu_2\rangle$ into BS, and the outputs $|\mu_{1+2}\rangle$ and $|\mu_{1-2}\rangle$ can be derived as follows:

$$\begin{aligned}
 |\mu_1\rangle|\mu_2\rangle &= |\sqrt{v}e^{i\alpha}\rangle_R|\sqrt{v}e^{i\beta}\rangle_R \\
 \xrightarrow{BS} &|\sqrt{\frac{v}{2}}(e^{i\alpha} + e^{i\beta})\rangle_R|\sqrt{\frac{v}{2}}(e^{i\alpha} - e^{i\beta})\rangle_R \\
 &= |\sqrt{2v}e^{i\frac{\alpha+\beta}{2}}\cos\frac{\alpha-\beta}{2}\rangle_R|\sqrt{2v}e^{i\frac{\alpha+\beta+\pi}{2}}\sin\frac{\alpha-\beta}{2}\rangle_R \\
 &= |\mu_{1+2}\rangle|\mu_{1-2}\rangle.
 \end{aligned} \tag{2}$$

Similarly, $|\mu_{3+4}\rangle$ and pulse $|\mu_{3-4}\rangle$ can be written as:

$$|\mu_{3+4}\rangle = |\sqrt{2v}e^{i\frac{\gamma+\delta}{2}}\cos\frac{\gamma-\delta}{2}\rangle_L, \tag{3}$$

$$|\mu_{3-4}\rangle = |\sqrt{2v}e^{i\frac{\gamma+\delta+\pi}{2}}\sin\frac{\gamma-\delta}{2}\rangle_L. \tag{4}$$

The pulses $|\mu_{1+2}\rangle$ and $|\mu_{3+4}\rangle$ are used to obtain the source information for post-selection. The pulses $|\mu_{1-2}\rangle$ and $|\mu_{3-4}\rangle$ continue to be fed into CPBS for combination. Notice that the CPBS here transmits the quantum state $|R\rangle$ and reflects the quantum state $|L\rangle$. After this, the

output can be derived as follows:

$$\begin{aligned}
 &|\mu_{1-2}\rangle|\mu_{3-4}\rangle \xrightarrow{PBS} |\mu_{1-2+3-4}\rangle \\
 &= |\sqrt{2v}e^{i\frac{\alpha+\beta+\pi}{2}}\sin\frac{\alpha-\beta}{2}\rangle_R|\sqrt{2v}e^{i\frac{\gamma+\delta+\pi}{2}}\sin\frac{\gamma-\delta}{2}\rangle_L \\
 &= \exp(-v\sin^2\frac{\alpha-\beta}{2})\exp(\sqrt{2v}e^{i\frac{\alpha+\beta+\pi}{2}}\sin\frac{\alpha-\beta}{2}a_R^\dagger) \\
 &\quad \exp(-\sqrt{2v}e^{-i\frac{\alpha+\beta+\pi}{2}}\sin\frac{\alpha-\beta}{2}a_R)\exp(-v\sin^2\frac{\gamma-\delta}{2}) \\
 &\quad \exp(\sqrt{2v}e^{i\frac{\gamma+\delta+\pi}{2}}\sin\frac{\gamma-\delta}{2}a_L^\dagger) \\
 &\quad \exp(-\sqrt{2v}e^{-i\frac{\gamma+\delta+\pi}{2}}\sin\frac{\gamma-\delta}{2}a_L)|vac\rangle \\
 &= \exp(-v(\sin^2\frac{\alpha-\beta}{2} + \sin^2\frac{\gamma-\delta}{2})) \\
 &\quad \exp(\sqrt{2v}e^{i\frac{\alpha+\beta+\pi}{2}}(\sin\frac{\alpha-\beta}{2}a_R^\dagger + e^{i(\frac{\gamma+\delta}{2} - \frac{\alpha+\beta}{2})}\sin\frac{\gamma-\delta}{2}a_L^\dagger)) \\
 &\quad \exp(-\sqrt{2v}e^{-i\frac{\alpha+\beta+\pi}{2}}(\sin\frac{\alpha-\beta}{2}a_R + e^{-i(\frac{\gamma+\delta}{2} - \frac{\alpha+\beta}{2})}\sin\frac{\gamma-\delta}{2}a_L))|vac\rangle.
 \end{aligned} \tag{5}$$

Here, we make some substitutions, as follows:

$$\begin{aligned}
 I_l &= 2v(\sin^2\frac{\alpha-\beta}{2} + \sin^2\frac{\gamma-\delta}{2}), \\
 \cos\frac{\theta}{2} &= \sin\frac{\alpha-\beta}{2}/\sqrt{\sin^2\frac{\alpha-\beta}{2} + \sin^2\frac{\gamma-\delta}{2}}, \\
 \sin\frac{\theta}{2} &= \sin\frac{\gamma-\delta}{2}/\sqrt{\sin^2\frac{\alpha-\beta}{2} + \sin^2\frac{\gamma-\delta}{2}}, \\
 \psi &= \frac{\gamma+\delta+\pi}{2}, \\
 \phi &= \frac{\gamma+\delta}{2} - \frac{\alpha+\beta}{2}, \\
 a^\dagger(\theta, \phi) &= \cos\frac{\theta}{2}a_R^\dagger + e^{i\psi}\sin\frac{\theta}{2}a_L^\dagger.
 \end{aligned} \tag{6}$$

Finally, the coherent pulse $|\mu_{1-2+3-4}\rangle$ is attenuated to $|\mu_{out}\rangle$ by BS, and

$$\begin{aligned}
 |\mu_{out}\rangle &= e^{-\frac{t}{2}}e^{\sqrt{t}Ie^{i\psi}a^\dagger(\theta, \phi)}e^{-\sqrt{t}Ie^{-i\psi}a(\theta, \phi)}|vac\rangle \\
 &= |\sqrt{t}Ie^{i\psi}\rangle_{a^\dagger(\theta, \phi)},
 \end{aligned} \tag{7}$$

where $I = tI_l$ and t is the transmission coefficient of BS. Through post-selection, we can define the polarization state intervals and decoy state intensity intervals as

$$\begin{aligned}
 S_x^y &= \{ \phi \in (\phi_x - \Delta\phi, \phi_x + \Delta\phi), \\
 &\quad \theta \in (\frac{\pi}{2} - \Delta\theta, \frac{\pi}{2} + \Delta\theta), \\
 &\quad y \in \{vac, d, s\} \}.
 \end{aligned} \tag{8}$$

When the transmitted states $|x\rangle$ are $|H\rangle$, $|V\rangle$, $|+\rangle$, and $|-\rangle$, ϕ_x corresponds to $0, \pi, \frac{\pi}{2}, \frac{3\pi}{2}$. And vac, d, s represent three decoy state intensity intervals where $s \in (I_d, I_s)$, $d \in (I_{vac}, I_d)$, $vac \in [0, I_{vac}]$, I_{vac}, I_d , and I_s are the boundaries of three intervals.

B. Photon transmission efficiency

In the whole system, photons are mainly lost by quantum channels, optical devices, and photon detector. Here, we consider the first two factors, which the photon detector will analyze in the next subsection. QSDC requires two rounds of transmission. Here, we write the first round of Bob to Alice as BA , and the second round of Alice to Bob as BAB . Then, the transmission efficiency of the system can be written as

$$\eta^{chan} = t^{chan} \eta_{opt}^{chan} \eta_m, \quad (9)$$

where $chan \in \{BA, BAB\}$, t^{chan} is the channel transmission efficiency, η_{opt}^{chan} is the intrinsic optical efficiency of the devices, and η_m is the efficiency of quantum memory.

Considering the most common fiber loss channels, t^{chan} can be further written as

$$t^{chan} = 10^{-\frac{\alpha^{chan}}{10}}, \quad (10)$$

where α^{chan} is quantum channel attenuation corresponding to the transmission round.

C. overall gain Q and error rate E

Next, we need to estimate overall gain Q and error rate E based on the model. Let's take Z base as an example. First, we consider the fully passive source to be an imperfect coherent source, whose photon number distribution follows the Poisson distribution $P_I(n)$ where $P_I(n) = e^{-I} \frac{I^n}{n!}$, and whose photons are in the quantum state $a^\dagger(\theta, \phi)$. Here we define the probability that n photons arrive at the detector as P_n and P_n is shown as follows

$$\begin{aligned} P_n &= \sum_{k=n}^{\infty} P_I(k) S(k, n) \\ &= \sum_{k=n}^{\infty} e^{-I} \frac{I^k}{k!} C_k^n (1 - \eta^{chan})^{k-n} (\eta^{chan})^n \\ &= \sum_{k=n}^{\infty} e^{-I} \frac{I^k}{k!} \frac{k!}{(k-n)!n!} (1 - \eta^{chan})^{k-n} (\eta^{chan})^n \\ &\xrightarrow{t=k-n} \sum_{t=0}^{\infty} I^n e^{-I} \frac{I^t}{t!n!} (1 - \eta^{chan})^t (\eta^{chan})^n \\ &= \frac{(I\eta^{chan})^n}{n!} e^{-I\eta^{chan}}, \end{aligned} \quad (11)$$

where $S(k, n)$ represents that the source emits k photons and n photons arrive at the detector.

When the n photons arrive at the detector, we have

$$\begin{aligned} |n\rangle_{a^\dagger(\theta, \phi)} &= \frac{1}{\sqrt{n!}} (a^\dagger(\theta, \phi))^n |vac\rangle \\ &= \frac{1}{\sqrt{n!}} \left(\frac{x_H}{\sqrt{2}} e^{i\Omega_H} a_H^\dagger + \frac{x_V}{\sqrt{2}} e^{i\Omega_V} a_V^\dagger \right)^n |vac\rangle \\ &= \frac{1}{\sqrt{n!}} \sum_{m=0}^n C_n^m \left(\frac{x_H}{\sqrt{2}} e^{i\Omega_H} a_H^\dagger \right)^m \left(\frac{x_V}{\sqrt{2}} e^{i\Omega_V} a_V^\dagger \right)^{n-m} |vac\rangle \\ &= \frac{1}{\sqrt{n!}} \sum_{m=0}^n C_n^m \left(\frac{x_H}{\sqrt{2}} e^{i\Omega_H} \right)^m \left(\frac{x_V}{\sqrt{2}} e^{i\Omega_V} \right)^{n-m} \\ &\quad \sqrt{m!(n-m)!} |m\rangle_H |n-m\rangle_V. \end{aligned} \quad (12)$$

Notice that

$$\begin{aligned} a^\dagger(\theta, \phi) &= \cos \frac{\theta}{2} a_R^\dagger + e^{i\phi} \sin \frac{\theta}{2} a_L^\dagger \\ &= \frac{1}{\sqrt{2}} (\cos \frac{\theta}{2} + e^{i\phi} \sin \frac{\theta}{2}) a_H^\dagger + \frac{i}{\sqrt{2}} (\cos \frac{\theta}{2} - e^{i\phi} \sin \frac{\theta}{2}) a_V^\dagger \\ &= \frac{1}{\sqrt{2}} (x_H e^{i\Omega_H} a_H^\dagger + x_V e^{i\Omega_V} a_V^\dagger) \\ &= \frac{1+i}{2} (\cos \frac{\theta}{2} - i e^{i\phi} \sin \frac{\theta}{2}) a_+^\dagger + \frac{1-i}{2} (\cos \frac{\theta}{2} + i e^{i\phi} \sin \frac{\theta}{2}) a_-^\dagger \\ &= \frac{1+i}{2} x_+ e^{i\Omega_+} a_+^\dagger + \frac{1-i}{2} x_- e^{i\Omega_-} a_-^\dagger \end{aligned} \quad (13)$$

and

$$\begin{aligned} x_H &= \sqrt{1 + \sin\theta \cos\phi}, \sin\Omega_H = \frac{\sin\phi \sin \frac{\theta}{2}}{x_H}, \\ x_V &= \sqrt{1 - \sin\theta \cos\phi}, \sin\Omega_V = \frac{-\sin\phi \sin \frac{\theta}{2}}{x_V}, \\ x_+ &= \sqrt{1 + \sin\theta \sin\phi}, \sin\Omega_+ = \frac{-\cos\phi \sin \frac{\theta}{2}}{x_+}, \\ x_- &= \sqrt{1 - \sin\theta \sin\phi}, \sin\Omega_- = \frac{\cos\phi \sin \frac{\theta}{2}}{x_-}. \end{aligned} \quad (14)$$

Then, the probability that the two detectors D_H and D_V receive $(m, n-m)$ photons respectively under the Z base is

$$P_{HV}(m, n-m) = C_n^m \left(\frac{x_H^2}{2} \right)^m \left(\frac{x_V^2}{2} \right)^{n-m}. \quad (15)$$

In this way, the probability that n photons arrive at detector and cause the detector D_H to respond can be

expressed as

$$\begin{aligned}
P_H^n &= \sum_{m=0}^n P_{HV}(m, n-m)[1 - (1 - \eta_H)^m(1 - Pd)] \quad (16) \\
&= \sum_{m=0}^n C_n^m \left(\frac{x_H^2}{2}\right)^m \left(\frac{x_V^2}{2}\right)^{n-m} [1 - (1 - \eta_H)^m(1 - Pd)] \\
&= \sum_{m=0}^n C_n^m \left(\frac{x_H^2}{2}\right)^m \left(\frac{x_V^2}{2}\right)^{n-m} (1 - \eta_V)^{n-m} (1 - Pd) - \\
&= \sum_{m=0}^n C_n^m \left(\frac{x_H^2}{2}\right)^m \left(\frac{x_V^2}{2}\right)^{n-m} (1 - \eta_V)^{n-m} (1 - Pd) - \\
&= \sum_{m=0}^n C_n^m \left(\frac{x_H^2}{2}\right)^m \left(\frac{x_V^2}{2}\right)^{n-m} (1 - \eta_V)^{n-m} (1 - Pd)^2 \\
&= (1 - Pd) \left(\frac{x_H^2}{2} + \frac{x_V^2}{2}(1 - \eta_V)\right)^n - \\
&= (1 - Pd)^2 \left(\frac{x_H^2}{2}(1 - \eta_H) + \frac{x_V^2}{2}(1 - \eta_V)\right)^n \\
&= (1 - Pd) \left(1 - \frac{x_V^2}{2}\eta_V\right)^n - \\
&= (1 - Pd)^2 \left(1 - \frac{x_H^2}{2}\eta_H - \frac{x_V^2}{2}\eta_V\right)^n,
\end{aligned}$$

where $\eta_H(\eta_V)$ is the detection efficiency of the detector $D_H(D_V)$, and Pd is the dark count probability.

Similarly, the probability of detector D_V 's response can be expressed as

$$\begin{aligned}
P_V^n &= (1 - Pd) \left(1 - \frac{x_H^2}{2}\eta_H\right)^n - \quad (17) \\
&= (1 - Pd)^2 \left(1 - \frac{x_H^2}{2}\eta_H - \frac{x_V^2}{2}\eta_V\right)^n.
\end{aligned}$$

Then, the gain of the detector D_H and D_V can be calculated as

$$\begin{aligned}
Q_H^{chan} &= \sum_{n=0}^{\infty} P_n P_H^n \\
&= \sum_{n=0}^{\infty} \frac{(I\eta^{chan})^n}{n!} e^{-I\eta^{chan}} \left[(1 - Pd) \left(1 - \frac{x_V^2}{2}\eta_V\right)^n - \right. \\
&= (1 - Pd)^2 \left(1 - \frac{x_H^2}{2}\eta_H - \frac{x_V^2}{2}\eta_V\right)^n \left. \right] \\
&= (1 - Pd) e^{-I\eta^{chan} \frac{x_H^2}{2}\eta_H} - (1 - Pd)^2 e^{-I\eta^{chan} \left(\frac{x_H^2}{2}\eta_H + \frac{x_V^2}{2}\eta_V\right)} \\
Q_V^{chan} &= \sum_{n=0}^{\infty} P_n P_V^n \\
&= (1 - Pd) e^{-I\eta^{chan} \frac{x_V^2}{2}\eta_V} - (1 - Pd)^2 e^{-I\eta^{chan} \left(\frac{x_H^2}{2}\eta_H + \frac{x_V^2}{2}\eta_V\right)}.
\end{aligned}$$

Finally, the overall gain of the state $a^\dagger(\theta, \phi)$ can be expressed as

$$\begin{aligned}
Q^{chan} &= Q_H^{chan} + Q_V^{chan}, \quad (19) \\
E^{chan} &= \frac{e_d Q_H^{chan} + (1 - e_d) Q_V^{chan}}{Q^{chan}}, \quad (20)
\end{aligned}$$

under Z base. e_d is detector error rate.

However, what we are thinking about here is the response of a state. Due to the randomness of the source, the quantum state of its output will fluctuate in a range. So we need to integrate over the corresponding state interval and the corresponding intensity interval. Thus, the overall gain Q of the interval S_x^y can be calculated as

$$\langle Q^{chan} \rangle_{S_x^y} = \frac{1}{\langle P \rangle_{S_x^y}} \iiint_{S_x^y} (Q_H^{chan} + Q_V^{chan}) f(I, \theta, \phi) dI d\theta d\phi. \quad (21)$$

We can also calculate the qubit error rate E . Take H for example

$$\langle E^{chan} \rangle_{S_H^y} = \frac{1}{\langle P \rangle_{S_H^y}} \iiint_{S_H^y} \frac{e_d Q_H^{chan} + (1 - e_d) Q_V^{chan}}{Q_H^{chan} + Q_V^{chan}} f(I, \theta, \phi) dI d\theta d\phi. \quad (22)$$

where $f(I, \theta, \phi)$ is a probability density function with three parameters [73]. $\langle P \rangle_{S_H^y}$ is the probability of selecting the interval, which is used for normalization, and

$$\langle P \rangle_{S_x^y} = \iiint_{S_x^y} f(I, \theta, \phi) dI d\theta d\phi, \quad (23)$$

$$f(I, \theta, \phi) = f(I, \theta) f(\phi), \quad (24)$$

$$f(\phi) = \frac{1}{2\Delta\phi}, \quad (25)$$

$$f(I, \theta) = \frac{1}{vt\pi^2 \sqrt{1 - \frac{I}{2vt} \cos^2 \frac{\theta}{2}} \sqrt{1 - \frac{I}{2vt} \sin^2 \frac{\theta}{2}}} \quad (26)$$

More details in Appendix A.

D. The theoretical secrecy message capacity

(18) For the single-photon DL04 protocol, Pan et al.[18] derive a theoretical secrecy message capacity formula under coherent attacks and photon number splitting (PNS) attacks. As follows

$$\begin{aligned}
C_s &= Q_s^{BAB} [1 - h(E_s^{BAB})] - \{Q_{s,n=1}^{BAE} * h(2e_1^{BA}) + \\
&= Q_{s,n=2}^{BAE} * [\frac{1}{2}h(2e_2^{BA}) + \frac{1}{2}] + Q_{s,n \geq 3}^{BAE} * 1\}. \quad (27)
\end{aligned}$$

where Q_s^{BAB} and E_s^{BAB} represent the overall gain and qubit error rate of the signal states transmitted in the second round, respectively. Here Eve performs PNS attacks on signal pulses of three photons and above to steal all information of photons. For two-photon events, Eve first performs PNS attack to steal one photon, and then performs coherent attack that can steal $\frac{1}{2}h(2e_2^{BA}) + \frac{1}{2}$ information. For single-photon events, Eve performs coherent attack to steal $h(2e_1^{BA})$ information from the error. Where e_1^{BA} and e_2^{BA} represent the single-photon and two-photon error rates of the first round transmission, respectively. The function $h(x)$ is the binary Shannon entropy

with the form of $h(x) = -x \log_2(x) - (1-x) \log_2(1-x)$. $Q_{s,n=1}^{BAE}$, $Q_{s,n=2}^{BAE}$, and $Q_{s,n \geq 3}^{BAE}$ respectively represent the overall gain of the different photon numbers stolen by Eve in the first round transmission, and can be estimated with the following formula

$$\begin{aligned} Q_s^{BAE} &= \sum_{n=0}^{\infty} Q_{s,n}^{BAE} \\ &\leq \sum_{n=0}^{\infty} [Q_{s,n}^{BA} - P_I(n)Y_0^A] \max\{1, \frac{\gamma^E}{\gamma^A}\}, \end{aligned} \quad (28)$$

where γ^E is the overall transmission efficiency of Eve after Alice encodes her receiving photons, and γ^A is the overall transmission efficiency for photons received and then measured by Alice. Y_0^A is the zero-photon yield at Alice in the first transmission round.

Thus, in our protocol, the secrecy message capacity can be written as

$$\begin{aligned} C_s &= \langle Q^{BAB} \rangle_{S_x^y} [1 - h(\langle E^{BAB} \rangle_{S_x^y})] - \{Q_{s,n=1}^{BAE} * h(2e_1^{BA}) \\ &\quad + Q_{s,n=2}^{BAE} * [\frac{1}{2}h(2e_2^{BA}) + \frac{1}{2}] + Q_{s,n \geq 3}^{BAE} * 1\}, \end{aligned} \quad (29)$$

$$\begin{aligned} Q_s^{BAE} &= \sum_{n=0}^{\infty} Q_{s,n}^{BAE} \\ &\leq \sum_{n=0}^{\infty} [(Q_n^{BA})_{S_x^y} - \langle P_I(n) \rangle_{S_x^y} Y_0^A] \max\{1, \frac{\gamma^E}{\gamma^A}\}, \end{aligned} \quad (30)$$

$$\langle Q_n^{BA} \rangle_{S_x^y} = \langle P_I(n) \rangle_{S_x^y} \langle Y_n \rangle_{S_x^y}, \quad (31)$$

$$\langle P_I(n) \rangle_{S_x^y} = \iiint_{S_H^y} e^{-I} \frac{I^n}{n!} f(I, \theta, \phi) dI d\theta d\phi. \quad (32)$$

E. Decoy state method

In section III.C, we give the formulas for calculating Q and E. In order to estimate the secrecy message capacity,

we also need to estimate e_1 and e_2 with decoy state. In reference [72], a method for solving e_1 and Y_1 using linear programming is given. To calculate e_1 and Y_1 , we need to solve the following linear programming problems

$$\begin{aligned} \min \quad & \langle Y_1 \rangle_{S_x} \\ \text{s.t.} \quad & \langle Q^{chan} \rangle_{S_x^y} \geq \sum_{n=0}^{n_{cut}} \langle P_I(n) \rangle_{S_x^y} \langle Y_n \rangle_{S_x}, \\ & \langle Q^{chan} \rangle_{S_x^y} \leq \sum_{n=0}^{n_{cut}} \langle P_I(n) \rangle_{S_x^y} \langle Y_n \rangle_{S_x} + 1 - \sum_{n=0}^{n_{cut}} \langle P_I(n) \rangle_{S_x^y}, \\ & 0 \leq \langle Y_n \rangle_{S_x} \leq 1. \\ & \max \langle e_1 Y_1 \rangle_{S_x} \\ \text{s.t.} \quad & \langle Q^{chan} E^{chan} \rangle_{S_x^y} \geq \sum_{n=0}^{n_{cut}} \langle P_I(n) \rangle_{S_x^y} \langle e_n Y_n \rangle_{S_x}, \\ & \langle Q^{chan} E^{chan} \rangle_{S_x^y} \leq \sum_{n=0}^{n_{cut}} \langle P_I(n) \rangle_{S_x^y} \langle e_n Y_n \rangle_{S_x} \\ & \quad + 1 - \sum_{n=0}^{n_{cut}} \langle P_I(n) \rangle_{S_x^y}, \\ & 0 \leq \langle e_n Y_n \rangle_{S_x} \leq 1. \end{aligned} \quad (33)$$

Since $\langle Y_n \rangle_{S_x^y}$ and $\langle e_n Y_n \rangle_{S_x^y}$ are independent of light intensity, we omit the superscript y which represents intensity in the interval. For the details of integral, see Appendix B.

In our previous work [71], we further propose the following linear programming problem to solve $\langle Y_2 \rangle_{S_x}$ and $\langle e_2 \rangle_{S_x}$.

$$\begin{aligned} \min \quad & \langle Y_2 \rangle_{S_x} \\ \text{s.t.} \quad & \langle P_I(1) \rangle_{S_x^i} \langle Q \rangle_{S_x^j} - \langle P_I(1) \rangle_{S_x^j} \langle Q \rangle_{S_x^i} \geq \langle Y_0 \rangle_{S_x} (\langle P_I(0) \rangle_{S_x^j} \langle P_I(1) \rangle_{S_x^i} - \langle P_I(0) \rangle_{S_x^i} \langle P_I(1) \rangle_{S_x^j}) \\ & \quad + \sum_{n=2}^{n_{cut}} \langle Y_n \rangle_{S_x} (\langle P_I(n) \rangle_{S_x^j} \langle P_I(1) \rangle_{S_x^i} - \langle P_I(n) \rangle_{S_x^i} \langle P_I(1) \rangle_{S_x^j}), \\ & \langle P_I(1) \rangle_{S_x^i} \langle Q \rangle_{S_x^j} - \langle P_I(1) \rangle_{S_x^j} \langle Q \rangle_{S_x^i} \leq \langle Y_0 \rangle_{S_x} (\langle P_I(0) \rangle_{S_x^j} \langle P_I(1) \rangle_{S_x^i} - \langle P_I(0) \rangle_{S_x^i} \langle P_I(1) \rangle_{S_x^j}) \\ & \quad + \sum_{n=2}^{n_{cut}} \langle Y_n \rangle_{S_x} (\langle P_I(n) \rangle_{S_x^j} \langle P_I(1) \rangle_{S_x^i} - \langle P_I(n) \rangle_{S_x^i} \langle P_I(1) \rangle_{S_x^j}) \\ & \quad + [\langle P_I(1) \rangle_{S_x^i} (1 - \sum_{n=0}^{n_{cut}} \langle P_I(n) \rangle_{S_x^j}) - \langle P_I(1) \rangle_{S_x^j} (1 - \sum_{n=0}^{n_{cut}} \langle P_I(n) \rangle_{S_x^i})], \\ & 0 \leq \langle Y_n \rangle_{S_x} \leq 1. \end{aligned} \quad (35)$$

$$\begin{aligned}
& \max \langle e_2 Y_2 \rangle_{S_x} \\
& \text{s.t.} \langle P_I(1) \rangle_{S_x^i} \langle E \rangle_{S_x^j} \langle Q \rangle_{S_x^j} - \langle P_I(1) \rangle_{S_x^j} \langle E \rangle_{S_x^i} \langle Q \rangle_{S_x^i} \geq \langle e_0 Y_0 \rangle_{S_x} (\langle P_I(0) \rangle_{S_x^j} \langle P_I(1) \rangle_{S_x^i} - \langle P_I(0) \rangle_{S_x^i} \langle P_I(1) \rangle_{S_x^j}) \\
& \quad + \sum_{n=2}^{n_{cut}} \langle e_n Y_n \rangle_{S_x} (\langle P_I(n) \rangle_{S_x^j} \langle P_I(1) \rangle_{S_x^i} - \langle P_I(n) \rangle_{S_x^i} \langle P_I(1) \rangle_{S_x^j}), \\
& \langle P_I(1) \rangle_{S_x^i} \langle E \rangle_{S_x^j} \langle Q \rangle_{S_x^j} - \langle P_I(1) \rangle_{S_x^j} \langle E \rangle_{S_x^i} \langle Q \rangle_{S_x^i} \leq \langle e_0 Y_0 \rangle_{S_x} (\langle P_I(0) \rangle_{S_x^j} \langle P_I(1) \rangle_{S_x^i} - \langle P_I(0) \rangle_{S_x^i} \langle P_I(1) \rangle_{S_x^j}) \\
& \quad + \sum_{n=2}^{n_{cut}} \langle e_n Y_n \rangle_{S_x} (\langle P_I(n) \rangle_{S_x^j} \langle P_I(1) \rangle_{S_x^i} - \langle P_I(n) \rangle_{S_x^i} \langle P_I(1) \rangle_{S_x^j}) \\
& \quad + [\langle P_I(1) \rangle_{S_x^i} (1 - \sum_{n=0}^{n_{cut}} \langle P_I(n) \rangle_{S_x^j}) - \langle P_I(1) \rangle_{S_x^j} (1 - \sum_{n=0}^{n_{cut}} \langle P_I(n) \rangle_{S_x^i})], \\
& 0 \leq \langle e_n Y_n \rangle_{S_x} \leq 1.
\end{aligned} \tag{36}$$

The two-photon component of QSDC also generates security message. In this way, we can estimate the secrecy message capacity of QSDC more accurately.

IV. NUMERICAL SIMULATION

In this section, we perform numerical simulations of our fully passive QSDC protocol. The parameters used are from the Pan's experiment [18], shown as Tab. 1.

TABLE I. Parameters used in the numerical simulation.

η_{opt}^{BA}	η_{opt}^{BAB}	Pd	e_d^A	e_d^B	$\eta_H(v)$
0.21	0.088	$8 * 10^{-8}$	0.0131	0.0026	0.7

Fig. 3 illustrates the secrecy message capacity versus the channel attenuation under the collective attack as well as the PNS attack in the framework of decoy-state analysis. We compared the fully passive QSDC under different intervals. We set $\Delta\phi = \Delta\theta = \Delta$, and the boundaries of three decoy-state intervals are $I_{vac} = 0.05I$, $I_d = 0.1I$, and $I_s = I$. These curves can be grouped in threes. Under identical intensity conditions, such as the red (3.1), blue (3.2), and green (3.3) curves, it is evident that a smaller interval Δ corresponds to a greater secrecy message capacity, enabling longer communication distances. This is because the size of the interval influences the quantum state generated by the fully passive source and a smaller interval produces a more accurate quantum state, thereby reducing the error rate. When considering equal interval sizes, the pulse does not consistently improve as intensity decreases, as illustrated by the red (3.1), orange (2.1), and pink (1.1) curves. It is evident that as intensity diminishes, the secrecy message capacity at short distances decreases. This reduction occurs because lower intensity leads to an increase in the vacuum state components produced by the source, thereby reducing the overall gain. Meanwhile, the decrease in intensity results in a lower probability of emitting multiple

photons, which can mitigate eavesdropping and extend the communication distance. However, when the advantages of multi-photon contributions are outweighed by the disadvantages of the vacuum state, the performance of the protocol begins to decline as light intensity increases. Therefore, selecting an appropriate intensity is crucial for optimizing the performance of the protocol.

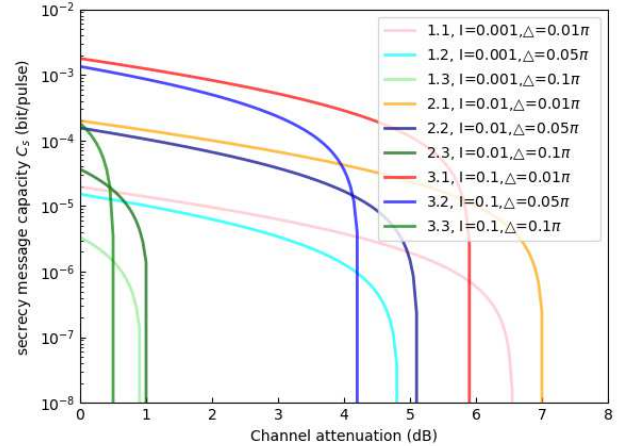


FIG. 3. Comparison of the fully passive QSDC with different I , $\Delta\phi$ and $\Delta\theta$. Here we set $\Delta\phi = \Delta\theta = \Delta$. We examined three intensities and three intervals, resulting in a total of nine curves. Depending on the parameters, these curves can be compared in groups of three.

In Fig. 4, we perform parameter optimization for the fully passive QSDC to find the optimal intensity for each channel attenuation to achieve the best secrecy message capacity. It is compared with the optimal case of active-modulated QSDC, and the optimal intensity of each channel attenuation is given in Fig. 5. The red, blue and green curves correspond to the case of $\Delta\phi = \Delta\theta = \Delta = 0.01\pi, 0.05\pi$ and 0.1π , respectively. As illustrated in Fig. 4, a reduction in interval size signifi-

cantly enhances the secrecy message capacity and transmission distance of the protocol. When the interval is sufficiently small, the performance of the fully passive QSDC approaches that of actively modulated QSDC. Its maximum communication distance is approximately 17.5 km (channel attenuation 7db). At a channel attenuation of 2, 4, 6 dB (corresponding to a communication distance of 5, 10, 15 km), the secrecy message capacity of fully passive QSDC with the interval of $\Delta\phi = \Delta\theta = 0.01\pi$ (the red curve) reaches 1.34×10^{-3} ($I = 0.266$), 3.10×10^{-4} ($I = 0.138$), and 2.81×10^{-5} ($I = 0.0474$) bit/pulse, achieving 78.0%, 75.7%, 69.2% of the active-modulated QSDC's performance (the black curve).

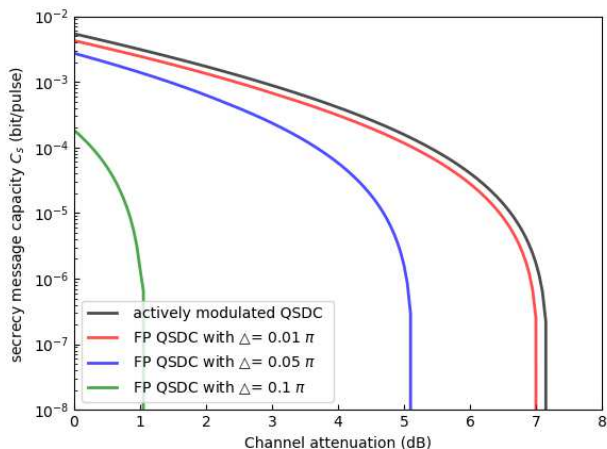


FIG. 4. Comparison between fully passive QSDC and active-modulated QSDC at the optimal intensities. We set $\Delta\phi = \Delta\theta = \Delta$. Among them, each channel attenuation corresponds to the secrecy message capacity under the optimal intensity. The optimal light intensity parameters are shown in Fig. 6. The red, blue, and green curves correspond to fully passive QSDC with interval sizes $\Delta = 0.01\pi, 0.05\pi$ and 0.1π , respectively. The black curve represents the active-modulated QSDC.

To optimize pulse performance, it is essential to achieve the smallest possible interval. However, this demands precise post-selection. The probability of post-selection is described by Eq. (23). While reducing the interval size can lower the error rate, it also requires substantial resources, consequently diminishing the amount of information transmitted per unit time. Therefore, considering practical applications, we optimize the interval size, resulting in an optimal secrecy message transmission rate when the pulse frequency of the light source is set at 10^6 Hz. In Fig. 6, the red curve shows the optimal secrecy message transmission rate when the memory efficiency η_m is equal to 1. The maximum communication distance of the protocol is approximately 17.75 km. At communication distances of 5 km and 10 km, the maximum secrecy message transmission rates are 10.268 bit/s

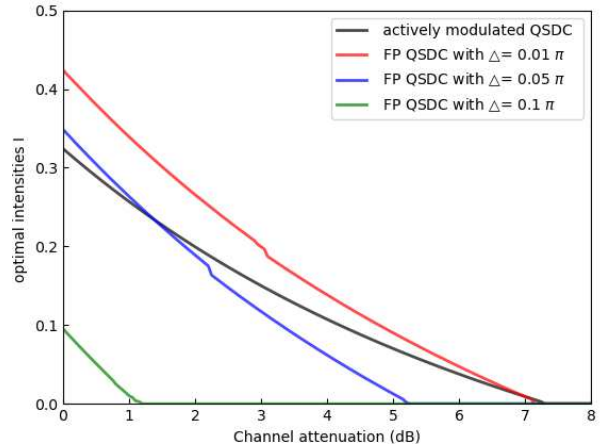


FIG. 5. The optimal intensities of fully passive QSDC and active-modulated QSDC. We set $\Delta\phi = \Delta\theta = \Delta$. The red, blue, and green curves correspond to the optimal intensities of fully passive QSDC with interval sizes $\Delta = 0.01\pi, 0.05\pi$ and 0.1π , respectively. The black curve correspond to the optimal intensities of active-modulated QSDC.

and 1.351 bit/s, respectively. The corresponding optimal parameters are presented in Table 2. Additionally, we examine the performance of the protocol under different memory efficiency conditions. The orange, blue, and green curves in Fig. 6 represent the secrecy message transmission rates with memory efficiencies of 0.95, 0.90, and 0.80, respectively. The optimal parameters corresponding to these efficiencies are shown in Fig. 7, Fig. 8, and Fig. 9. Specific values for the secrecy message transmission rates and the corresponding optimal parameters at 5 km and 10 km are also provided in Table 2.

TABLE II. At communication distances of 5 and 10 km, the optimal secrecy message transmission rate of the protocol corresponding to different memory efficiency η_m and the corresponding optimal parameters $\Delta\theta, \Delta\phi, I$ are obtained.

η_m	L(km)	$\Delta\theta(\pi)$	$\Delta\phi(\pi)$	I	C (bit/sec)
1	5	5.092×10^{-2}	5.088×10^{-2}	1.861×10^{-1}	10.268
0.95	5	4.852×10^{-2}	4.846×10^{-2}	1.567×10^{-1}	7.232
0.9	5	4.540×10^{-2}	4.537×10^{-2}	1.376×10^{-1}	4.904
0.8	5	3.854×10^{-2}	3.842×10^{-2}	9.971×10^{-2}	1.853
1	10	3.802×10^{-2}	3.799×10^{-2}	9.570×10^{-2}	1.351
0.95	10	3.484×10^{-2}	3.475×10^{-2}	8.146×10^{-2}	8.119×10^{-1}
0.9	10	3.151×10^{-2}	3.130×10^{-2}	6.713×10^{-2}	4.388×10^{-1}
0.8	10	2.209×10^{-2}	2.258×10^{-2}	3.852×10^{-2}	6.982×10^{-2}

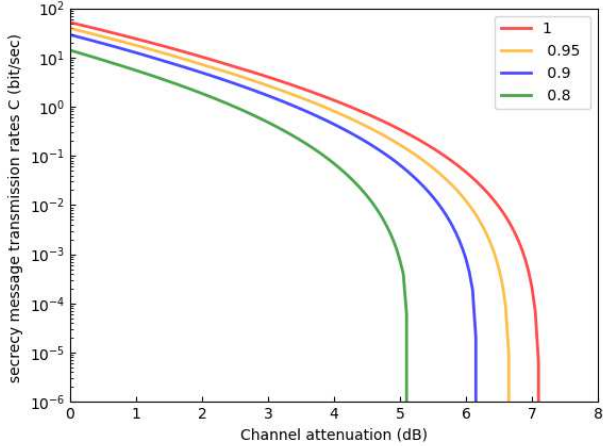


FIG. 6. The optimal secrecy message transmission rates of fully passive QSDC. The pulse frequency of coherent source is 10^6 Hz. The red, orange, blue, and green curves correspond to protocol performance when the memory efficiency is 1, 0.95, 0.9, and 0.8, respectively. The optimal parameters I , $\Delta\theta$ and $\Delta\phi$, are given in Fig.8, Fig.9 and Fig.10 respectively.

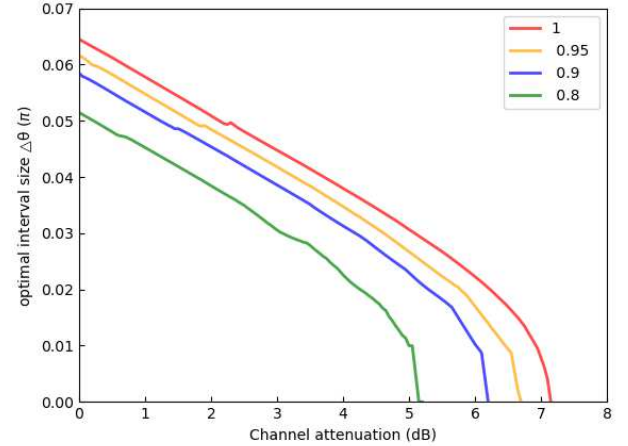


FIG. 8. The optimal intervals $\Delta\theta$ of fully passive QSDC. The red, orange, blue, and green curves correspond to the optimal intervals $\Delta\theta$ when the memory efficiency is 1, 0.95, 0.9, and 0.8, respectively.

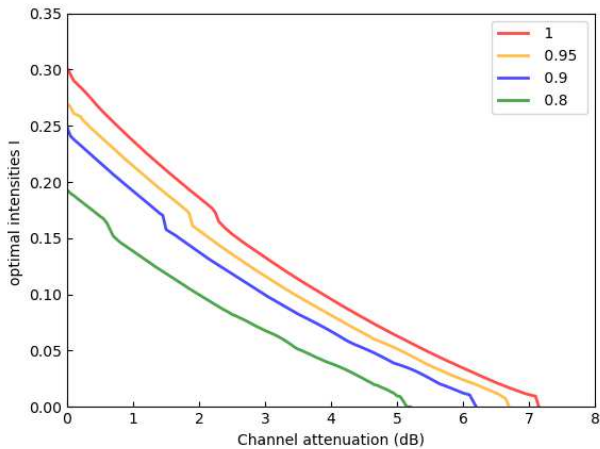


FIG. 7. The optimal intensities of fully passive QSDC. The red, orange, blue, and green curves correspond to the optimal intensities when the memory efficiency is 1, 0.95, 0.9, and 0.8, respectively.

V. CONCLUSION

In conclusion, we propose a fully passive QSDC protocol. Weakly coherent pulses with random intensity and random quantum state can be generated passively through the interference, beam combination and attenuation of four phase random coherent pulses. This passive modulation can not only reduce the experimental opera-

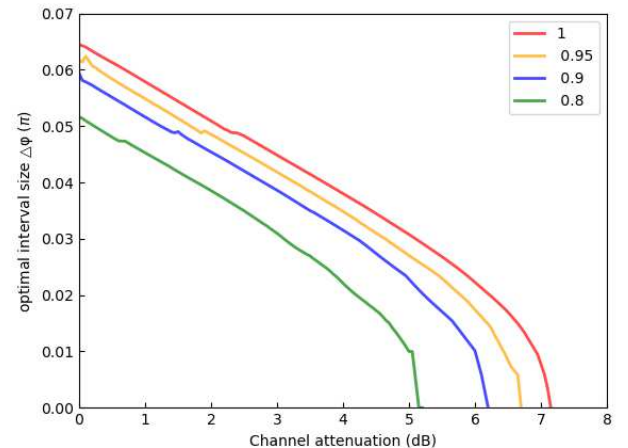


FIG. 9. The optimal intervals $\Delta\phi$ of fully passive QSDC. The red, orange, blue, and green curves correspond to the optimal intervals $\Delta\phi$ when the memory efficiency is 1, 0.95, 0.9, and 0.8, respectively.

tion, but also resist the side-channel attack of the third party against the source. In terms of security analysis, we conducted decoy-state analysis considering PNS attacks and coherent attacks of third-party Eve. At the same time, we optimize the parameters of fully passive QSDC to find the optimal input light intensity corresponding to each channel attenuation, and compare it with actively modulated QSDC. The results show that the performance of the protocol is close to that of QSDC. At a channel attenuation of 4 dB (corresponding to a

communication distance of 10 km), its secrecy message capacity is $3.10 * 10^{-4}$ bit/pulse ($I = 0.1380$), which is about 75.7% of the actively modulated QSDC. At a channel attenuation of 6 dB (corresponding to a communication distance of 15 km), its secrecy message capacity is $2.81 * 10^{-5}$ bit/pulse ($I = 0.0474$), which is about 69.2% of the actively modulated QSDC. We also examine resource consumption and memory efficiency, optimizing the post-selection intervals to determine the optimal secrecy message transmission rate and the corresponding post-selection interval size for each channel attenuation when the light source frequency is 10^6 Hz. In conclusion, our protocol combines a fully passive source with a QSDC, and gives a complete security analysis, which provides a reference for a more secure QSDC in practice.

VI. APPENDIX A: PROBABILITY DENSITY FUNCTION

Here we are talking about the probability density function, similar to [73]. First, we need an assumption that the initial four coherent pulse sources have phases that are uniform distribution over the domain. According to formula 6, we can easily see that ϕ is also uniform distribution over the domain. And we have

$$f(I, \theta, \phi) = f(I, \theta)f(\phi) \quad (37)$$

$$f(\phi) = \frac{1}{2\Delta\phi} \quad (38)$$

According to formula 6, let $\frac{\alpha-\beta}{2}=\theta_1$ and $\frac{\gamma-\delta}{2}=\theta_2$, we have

$$I = 2vt(\sin^2\theta_1 + \sin^2\theta_2) \quad (39)$$

$$\theta = 2\arctan\frac{\sin\theta_2}{\sin\theta_1}$$

$$\sin\theta_1 = \cos\frac{\theta}{2}\sqrt{\frac{I}{2vt}}$$

$$\sin\theta_2 = \sin\frac{\theta}{2}\sqrt{\frac{I}{2vt}}$$

Obviously, θ_1 and θ_2 are uniformly distributed. According to the transformation formula for random variables, we have

$$f(I, \theta) = \frac{1}{|J|}f(\theta_1, \theta_2) \quad (40)$$

where $|J|$ is Jacobian determinant, and

$$|J| = \left| \begin{array}{cc} \frac{\partial I}{\partial \theta_1} & \frac{\partial I}{\partial \theta_2} \\ \frac{\partial \theta}{\partial \theta_1} & \frac{\partial \theta}{\partial \theta_2} \end{array} \right| = 8vt\cos\theta_1\cos\theta_2 \quad (41)$$

$$= 8vt\sqrt{1 - \frac{I}{2vt}\cos^2\frac{\theta}{2}}\sqrt{1 - \frac{I}{2vt}\sin^2\frac{\theta}{2}} \quad (42)$$

$f(\theta_1, \theta_2)$ is a constant that depends on the domain. The value of θ_1 and θ_2 affect the domain of I and θ , but it

is difficult to use I and θ to backinfer the domain of θ_1 and θ_2 . Therefore, we retrodict the probability density function according to its normalization conditions. Thus

$$\int_{I=0}^{I=2vt} \int_{\theta=0}^{\theta=\pi} f(I, \theta)dId\theta = 1 \quad (43)$$

$$f(I, \theta) = \frac{1}{vt\pi^2\sqrt{1 - \frac{I}{2vt}\cos^2\frac{\theta}{2}}\sqrt{1 - \frac{I}{2vt}\sin^2\frac{\theta}{2}}} \quad (44)$$

and $I \in (0, 2vt), \theta \in (0, \pi)$.

VII. APPENDIX B: YIELD AND ERROR RATE

According to Eq. (16) and Eq. (17), we can calculate the theoretical value of $\langle Y_n \rangle_{S_x}$ as

$$Y_n = \sum_{k=0}^n C_n^k (1-\eta)^{n-k} \eta^k (P_H^k + P_V^k) \quad (45)$$

$$\begin{aligned} &= (1-Pd)[1 - \eta\eta_V \frac{1 - \sin\theta\cos\phi}{2}]^n + \\ & (1-Pd)[1 - \eta\eta_H \frac{1 + \sin\theta\cos\phi}{2}]^n - \\ & 2(1-Pd)^2[1 - \eta\eta_V \frac{1 - \sin\theta\cos\phi}{2} - \eta\eta_H \frac{1 + \sin\theta\cos\phi}{2}]^n \\ \langle Y_n \rangle_{S_x} &= \frac{1}{\langle P \rangle_{S_x^y}} \iiint_{S_x^y} Y_n f(I, \theta, \phi) dId\theta d\phi \quad (46) \end{aligned}$$

Since Y_n is only related to θ and ϕ , $P_I(n)$ is only related to I . In the way, the integral $\langle P_I(n)Y_n \rangle_{S_x^y}$ can be split into $\langle P_I(n) \rangle_{S_x^y} \langle Y_n \rangle_{S_x}$.

Similarly, taking state $|H\rangle$ as an example, the error can be calculated as

$$e_n Y_n = \sum_{k=0}^n C_n^k [e_d P_H^k + (1-e_d)P_V^k] \quad (47)$$

$$\begin{aligned} &= e_d(1-Pd)[1 - \eta\eta_V \frac{1 - \sin\theta\cos\phi}{2}]^n + \\ & (1-e_d)(1-Pd)[1 - \eta\eta_H \frac{1 + \sin\theta\cos\phi}{2}]^n - \\ & (1-Pd)^2[1 - \eta\eta_V \frac{1 - \sin\theta\cos\phi}{2} - \eta\eta_H \frac{1 + \sin\theta\cos\phi}{2}]^n \\ \langle e_n Y_n \rangle_{S_x} &= \frac{1}{\langle P \rangle_{S_x^y}} \iiint_{S_x^y} e_n Y_n f(I, \theta, \phi) dId\theta d\phi \quad (48) \end{aligned}$$

Similarly, $\langle P_I(n)e_n Y_n \rangle_{S_x^y}$ can be split into $\langle P_I(n) \rangle_{S_x^y} \langle e_n Y_n \rangle_{S_x}$. However, $\langle e_n Y_n \rangle_{S_x}$ is not equal to $\langle e_n \rangle_{S_x} \langle Y_n \rangle_{S_x}$, and the decoy state method can only obtain an estimate of $\langle e_n Y_n \rangle_{S_x}$. $\langle e_n \rangle_{S_x}$ cannot be obtained by directly calculating $\frac{\langle e_n Y_n \rangle_{S_x}}{\langle Y_n \rangle_{S_x}}$. So we have to revise our estimates as follows

$$\langle \hat{e}_n \rangle_{S_x} = \frac{\langle \widehat{e_n Y_n} \rangle_{S_x}}{\langle \hat{Y}_n \rangle_{S_x}} + \Delta \quad (49)$$

$$\Delta = \langle e_n \rangle_{S_x} - \frac{\langle e_n Y_n \rangle_{S_x}}{\langle Y_n \rangle_{S_x}} \quad (50)$$

where the mark $\hat{\cdot}$ represents the estimate of the decoy state method, and Δ can be obtained by integrating Eq. (45) and Eq. (47).

and No. 92365110.

ACKNOWLEDGEMENT

This work is supported by the National Natural Science Foundation of China under Grants No. 12175106

-
- [1] G. L. Long, and X. S. Liu, Theoretically efficient high-capacity quantum-key-distribution scheme, *Phys. Rev. A* **65**, 032302 (2002).
- [2] F. G. Deng, G. L. Long, and X. S. Liu, Two-step quantum direct communication protocol using the Einstein-Podolsky-Rosen pair block, *Phys. Rev. A* **68**, 042317 (2003).
- [3] F. G. Deng, and G. L. Long, Secure direct communication with a quantum one-time pad, *Phys. Rev. A* **69**, 052319 (2004).
- [4] C. Wang, F.G. Deng, Y.S. Li, X.S. Liu, and G.L. Long. Quantum secure direct communication with high-dimension quantum superdense coding. *Phys. Rev. A* **71** 044305 (2005).
- [5] T. Li, and G. L. Long, Quantum secure direct communication based on single-photon Bell-state measurement, *New J. Phys.* **22**, 063017 (2020).
- [6] G. L. Long, and H. Zhang, Drastic increase of channel capacity in quantum secure direct communication using masking, *Sci. Bull.* **66**, 1267-1269 (2021).
- [7] Y. B. Sheng, L. Zhou, and G. L. Long, One-step quantum secure direct communication, *Sci. Bull.* **67**, 367-374 (2022).
- [8] J. W. Wu, G. L. Long, and M. Hayashi, Quantum secure direct communication with private dense coding using a general preshared quantum state, *Phys. Rev. Appl.* **17**, 064011 (2022).
- [9] Y. X. Xiao, L. Zhou, W. Zhong, M. M. Du, and Y. B. Sheng, The hyperentanglement-based quantum secure direct communication protocol with single-photon measurement, *Quant. Inform. Process.* **22**, 339 (2023).
- [10] Q. Zhang, M. M. Du, W. Zhong, Y. B. Sheng, and L. Zhou, Single-photon based three-party quantum secure direct communication with identity authentication, *Ann. Phys. (Berlin, Ger.)* **536**, 3 (2024).
- [11] D. Pan, G. L. Long, L. G. Yin, Y. B. Sheng, D. Ruan, S. X. Ng, J. H. Lu, and L. Hanzo, The Evolution of Quantum Secure Direct Communication: On the Road to the Qinternet, *IEEE Communications Surveys & Tutorial* **26**, 1898-1949 (2024).
- [12] J. Y. Hu, B. Yu, M. Y. Jing, L. T. Xiao, S. T. Jia, G. Q. Qin, and G. L. Long, Experimental quantum secure direct communication with single photons, *Light: Sci. & Appl.* **5**, e16144 (2016).
- [13] W. Zhang, D. S. Ding, Y. B. Sheng, L. Zhou, B. S. Shi, and G. C. Guo, Quantum secure direct communication with quantum memory, *Phys. Rev. Lett.* **118**, 220501 (2017).
- [14] F. Zhu, W. Zhang, Y. B. Sheng, and Y. D. Huang, Experimental long-distance quantum secure direct communication, *Sci. Bull.* **10**, 1519-1524 (2017).
- [15] R. Qi, Z. Sun, Z. Lin, P. Niu, W. Hao, L. Song, Q. Huang, J. Gao, L. Yin, and G.-L. Long. Implementation and security analysis of practical quantum secure direct communication. *Light Sci. Appl.* **8**, 22 (2019).
- [16] Z. T. Qi, Y. H. Li, W. Y. Huang, J. Feng, Y. L. Zheng, and X. F. Chen, A 15-user quantum secure direct communication network, *Light: Sci. & Appl.* **10**, 183 (2021).
- [17] H. R. Zhang, Z. Sun, R. Y. Qi, L. G. Yin, G. L. Long, and J. H. Lu, Realization of quantum secure direct communication over 100 km fiber with time-bin and phase quantum states, *Light: Sci & Appl.* **11**, 83 (2022).
- [18] D. Pan, Z. Lin, J. Wu, H. Zhang, Z. Sun, D. Ruan, L. Yin, G.L. Long. Experimental free-space quantum secure direct communication and its security analysis. *Photonics Research* **8**, 9 (2020).
- [19] Z. Cao, L. Wang, K. Liang, G. Chai, and J. Peng. Continuous-variable quantum secure direct communication based on Gaussian mapping. *Phys. Rev. Appl.* **16** 024012 (2021).
- [20] Z. W. Cao, Y. Lu, G. Chai, H. Yu, K. X. Liang, and L. Wang, Realization of quantum secure direct communication with continuous variable, *Research* **6**, 0193 (2023).
- [21] E. Diamanti, H. K. Lo, B. Qi, and Z. L. Yuan, Practical challenges in quantum key distribution, *npj Quantum Information* **2**, 16025 (2016).
- [22] F. H. Xu, X. F. Ma, Q. Zhang, H. K. Lo, and J. W. Pan, Secure quantum key distribution with realistic devices, *Rev. Mod. Phys.* **92**, 025002 (2020).
- [23] M. Bozzio, M. Vyblecka, M. Cosacchi, C. Nawrath, T. Seidelmann, J. C. Loredó, S. L. Portalupi, V. M. Axt, P. Michler, and P. Walther, Enhancing quantum cryptography with quantum dot single-photon sources, *npj Quantum Information* **8**, 104 (2022).
- [24] J. Wu, Z. Lin, L. Yin, and G.-L. Long. Security of quantum secure direct communication based on Wyner's wiretap channel theory. *Quantum Eng.* **1**, e26 (2019).
- [25] R. Y. Qi, Z. Sun, Z. S. Lin, P. H. Niu, W. T. Hao, L. Y. Song, Q. Huang, J. C. Gao, L. G. Yin, and G. L. Long, Implementation and security analysis of practical quantum secure direct communication, *Light: Sci. Appl.* **8**, 22 (2019).
- [26] X. Liu, Z.J. Li, D. Luo, C.F. Huang, D. Ma, M.M. Geng, J.W. Wang, Z.R. Zhang, and K.J. Wei. Practical decoy-state quantum secure direct communication. *Sci. China: Phys. Mech. & Astron.* **64**, 120311 (2021).

- [27] G. Brassard, N. Lütkenhaus, T. Mor, and B. C. Sanders, Limitations on Practical Quantum Cryptography, *Phys. Rev. Lett.* **85**, 1330 (2000).
- [28] L. Lydersen, C. Wiechers, C. Wittmann, D. Elser, J. Skaar, and V. Makarov, Hacking commercial quantum cryptography systems by tailored bright illumination, *Nat. Photonics* **4**, 686-689 (2010).
- [29] I. Gerhardt, Q. Liu, A. L. Linares, J. Skaar, C. Kurtsiefer, and V. Makarov, Full-field implementation of a perfect eavesdropper on a quantum cryptography system, *Nat. Commun.* **2**, 349 (2011).
- [30] S. H. Sun, M. Gao, M. S. Jiang, C. Y. Li, and L. M. Liang, Partially random phase attack to the practical two-way quantum-key-distribution system, *Phys. Rev. A* **85**, 032304 (2012).
- [31] S. H. Sun, F. H. Xu, M. S. Jiang, X. C. Ma, H. K. Lo, and L. M. Liang, Effect of source tampering in the security of quantum cryptography, *Phys. Rev. A* **92**, 022304 (2015).
- [32] H. K. Lo, M. Curty, and B. Qi, Measurement-device-independent quantum key distribution, *Phys. Rev. Lett.* **108**, 130503 (2012).
- [33] Y. Liu, T. Y. Chen, L. J. Wang, H. Liang, G. L. Shen-tu, J. Wang, K. Cui, H. L. Yin, N. L. Liu, L. Li, X. F. Ma, J. S. Pelc, M. M. Fejer, C. Z. Peng, Q. Zhang, and J. W. Pan, Experimental Measurement-Device-Independent Quantum Key Distribution, *Phys. Rev. Lett.* **111**, 130502 (2013).
- [34] H. L. Yin, T. Y. Chen, Z. W. Yu, H. Liu, L. X. You, Y. H. Zhou, S. J. Chen, Y. Q. Mao, M. Q. Huang, W. J. Zhang, H. Chen, M. J. Li, D. Nolan, F. Zhou, X. Jiang, Z. Wang, Q. Zhang, X. B. Wang, and J. W. Pan, Measurement-Device-Independent Quantum Key Distribution Over a 404 km Optical Fiber, *Phys. Rev. Lett.* **117**, 190501 (2016).
- [35] Y. Cao, Y. H. Li, K. X. Yang, Y. F. Jiang, S. L. Li, X. L. Hu, M. Abulizi, C. L. Li, W. J. Zhang, Q. C. Sun, W. Y. Liu, X. Jiang, S. K. Liao, J. G. Ren, H. Li, L. X. You, Z. Wang, J. Yin, C. Y. Lu, X. B. Wang, Q. Zhang, C. Z. Peng, and J. W. Pan, Long-Distance Free-Space Measurement-Device-Independent Quantum Key Distribution, *Phys. Rev. Lett.* **125**, 260503 (2020).
- [36] D. Luo, X. Liu, K. B. Qin, Z. R. Zhang, and K. J. Wei, Practical asynchronous measurement-device-independent quantum key distribution with advantage distillation, *Phys. Rev. A* **110**, 022605 (2024).
- [37] P. H. Niu, Z. R. Zhou, Z. S. Lin, Y. B. Sheng, L. G. Yin, and G. L. Long, Measurement-device-independent quantum communication without encryption, *Sci. Bull.* **63**, 1345-1350 (2018).
- [38] Z. R. Zhou, Y. B. Sheng, P. H. Niu, L. G. Yin, G. L. Long, and L. Hanzo, Measurement-device-independent quantum secure direct communication, *Sci. China: Phys. Mech. & Astron.* **63**, 230362 (2020).
- [39] X. D. Wu, L. Zhou, W. Zhong, Y. B. Sheng, High-capacity measurement-device-independent quantum secure direct communication, *Quant. Inf. Process.* **19** 10354 (2020).
- [40] J. W. Ying, L. Zhou, W. Zhong, and Y. B. Sheng, Measurement-device-independent one-step quantum secure direct communication, *Chin. Phys. B* **31**, 120303 (2022).
- [41] Y. P. Hong, L. Zhou, W. Zhong, and Y. B. Sheng, Measurement-device-independent three-party quantum secure direct communication, *Quant. Inform. Process.* **22**, 111 (2023).
- [42] J. Liu, X. Zou, X. Wang, Y. Chen, Z. Rong, Z. Huang, S. Zheng, X. Liang, and J. Wu, Applying a class of general maximally entangled states in measurement-device-independent quantum secure direct communication, *Phys. Rev. Appl.* **21**, 044010 (2024).
- [43] A. Acín, N. Brunner, N. Gisin, S. Massar, S. Pironio, and V. Scarani, Device-independent security of quantum cryptography against collective attacks, *Phys. Rev. Lett.* **98**, 230501 (2007).
- [44] L. Zhou, Y. B. Sheng, and G. L. Long, Device-independent quantum secure direct communication against collective attacks, *Sci. Bull.* **65**, 12-20 (2020).
- [45] S. Pironio, A. Acín, N. Brunner, N. Gisin, S. Massar and V. Scarani, Device-independent quantum key distribution secure against collective attacks, *New J. Phys.* **11**, 045021 (2009).
- [46] J. Kolodyński, A. Máttar, P. Skrzypczyk, E. Woodhead, D. Cavalcanti, K. Banaszek, and A. Acín, Device-independent quantum key distribution with single-photon sources, *Quantum* **4**, 260 (2020).
- [47] L. Zhou, and Y. B. Sheng, One-step device-independent quantum secure direct communication, *Sci. China: Phys. Mech. & Astron.* **65**, 250311 (2022).
- [48] L. Zhou, B. W. Xu, W. Zhong, and Y. B. Sheng, Device-independent quantum secure direct communication with single-photon sources, *Phys. Rev. Appl.* **19**, 014036 (2023).
- [49] H. Zeng, M. M. Du, W. Zhong, L. Zhou, and Y. B. Sheng, High-capacity device-independent quantum secure direct communication based on hyper-encoding, *Funda. Res.* **4**, 852-858 (2024).
- [50] D. P. Nadlinger, P. Drmota, B. C. Nichol, G. Araneda, D. Main, R. Srinivas, D. M. Lucas, C. J. Ballance, K. Ivanov, and E. Z. Tan, Experimental quantum key distribution certified by Bell's theorem, *Nature* **607**, 682-686 (2022).
- [51] W. Zhang, T. V. Leent, K. Redeker, R. Garthoff, R. Schwonnek, F. Fertig, S. Eppelt, W. Rosenfeld, V. Scarani, and C. C. W. Lim, A device-independent quantum key distribution system for distant users, *Nature* **607**, 687-691 (2022).
- [52] W. Z. Liu, Y. Z. Zhang, Y. Z. Zhen, M. H. Li, Y. Liu, J. Y. Fan, F. H. Xu, Q. Zhang, and J. W. Pan, Toward a photonic demonstration of device-independent quantum key distribution, *Phys. Rev. Lett.* **129**, 050502 (2022).
- [53] I. W. Primaatmaja, K. T. Goh, E. Y.-Z. Tan, J. T.-F. Khoo, S. Ghorai, and C. Lim, Security of device-independent quantum key distribution protocols: a review, *Quantum*, **7**, 932 (2023).
- [54] H.K. Lo, X.F. Ma, and K. Chen, Decoy state quantum key distribution, *Phys. Rev. Lett.* **94**, 230504 (2005).
- [55] X.F. Ma, B. Qi, Y. Zhao, and H.K. Lo, Practical decoy state for quantum key distribution, *Phys. Rev. A* **72**, 012326 (2005).
- [56] A. Vakhitov, V. Makarov, and D. R. Hjelm, Large pulse attack as a method of conventional optical eavesdropping in quantum cryptography, *J. Mod. Opt.* **48**, 2023 (2001).
- [57] N. Gisin, S. Fasel, B. Kraus, H. Zbinden, and G. Ribordy, Trojan-horse attacks on quantum-key-distribution systems, *Phys. Rev. A* **73**, 022320 (2006).
- [58] Á. Navarrete, and M. Curty, Improved finite-key security analysis of quantum key distribution against Trojan-horse attacks, *Quantum Science and Technology*, **7**, 3

- (2022).
- [59] T. T. Luo, Q. Liu, X. R. Sun, C. F. Huang, Y. Chen, Z. R. Zhang, and K. J. Wei, Security analysis against the Trojan horse attack on practical polarization-encoding quantum key distribution systems, *Phys. Rev. A* **109**, 042608 (2024).
- [60] Q. Wang, C. H. Zhang, and X. B. Wang, Scheme for realizing passive quantum key distribution with heralded single-photon sources, *Phys. Rev. A* **93**, 032312 (2016).
- [61] C. H. Zhang, C. M. Zhang, and Q. Wang, Efficient passive measurement-device-independent quantum key distribution, *Phys. Rev. A* **99**, 052325 (2019).
- [62] M. Curty, T. Moroder, X. F. Ma, and N. Lütkenhaus, Non Poissonian statistics from Poissonian light sources with application to passive decoy state quantum key distribution, *Opt. Lett.* **34**, 3238-3240 (2009).
- [63] M. Curty, X. F. Ma, B. Qi, and T. Moroder, Passive decoy-state quantum key distribution with practical light sources, *Phys. Rev. A* **81**, 022310 (2010).
- [64] Q. C. Sun, W. L. Wang, Y. Liu, F. Zhou, J. S. Pelc, M. M. Fejer, C. Z. Peng, X. F. Chen, X. F. Ma, Q. Zhang, and J. W. Pan, Experimental passive decoy-state quantum key distribution, *Laser Phys. Lett.* **11**, 085202 (2014).
- [65] S. H. Sun, G. Z. Tang, C. Y. Li, and L. M. Liang, Experimental demonstration of passive decoy-state quantum key distribution with two independent lasers, *Phys. Rev. A* **94**, 032324 (2016).
- [66] J. W. Ying, P. Zhao, W. Zhong, M. M. Du, X. Y. Li, S. T. Shen, A. L. Zhang, L. Zhou, and Y. B. Sheng, Passive decoy-state quantum secure direct communication with heralded single-photon source, *Phys. Rev. Appl.* **22**, 024040 (2024).
- [67] M. Curty, X. F. Ma, H. K. Lo, and N. Lütkenhaus, Passive sources for the Bennett-Brassard 1984 quantum-key-distribution protocol with practical signals, *Phys. Rev. A* **82**, 052325 (2010).
- [68] B. Qi, P. G. Evans, and W. P. Grice, Passive state preparation in the Gaussian-modulated coherent-states quantum key distribution, *Phys. Rev. A* **97**, 012317 (2018).
- [69] B. Qi, H. Gunther, P. G. Evans, B. P. Williams, R. M. Camacho, and N. A. Peters, Experimental Passive-State Preparation for Continuous-Variable Quantum Communications, *Phys. Rev. Applied* **13**, 054065 (2020).
- [70] F. Y. Ji, P. Huang, T. Wang, X. Q. Jiang, and G. H. Zeng, Gbps key rate passive-state-preparation continuous-variable quantum key distribution within an access-network area, *Photonics Res.* **12**, 1485 (2024).
- [71] J. W. Ying, J. Y. Wang, Y. X. Xiao, S. P. Gu, X. F. Wang, W. Zhong, M. M. Du, X. Y. Li, S. T. Shen, A. L. Zhang, L. Zhou, and Y. B. Sheng, Passive-state preparation for quantum secure direct communication, *Sci. China: Phys. Mech. & Astron.* **68**, 240312 (2025).
- [72] W. Y. Wang, R. Wang, C. Q. Hu, V. Zapatero, L. Qian, B. Qi, M. Curty, and H. K. Lo, Fully passive quantum key distribution, *Phys. Rev. Lett.* **130**, 220801 (2023).
- [73] V. Zapatero, W. Wang, and M. Curty, A fully passive transmitter for decoy-state quantum key distribution, *Quantum Sci. Technol.* **8**, 025014 (2023).
- [74] V. Zapatero, and M. Curty, Finite-key security of passive quantum key distribution, *Phys. Rev. Appl.* **21**, 014018 (2024).
- [75] J. J. Li, W. Y. Wang, and H. K. Lo, Fully passive measurement-device-independent quantum key distribution, *Phys. Rev. Appl.* **21**, 064056 (2024).
- [76] X. Wang, F. Y. Lu, Z. H. Wang, Z. Q. Yin, S. Wang, J. Q. Geng, W. Chen, D. Y. He, G. C. Guo, and Z. F. Han, Fully passive measurement-device-independent quantum key distribution, *Phys. Rev. Appl.* **21**, 064067 (2024).
- [77] W. Y. Wang, R. Wang, and H. K. Lo, Fully-Passive Twin-Field Quantum Key Distribution, arXiv:2304.12062.
- [78] J. J. Li, W. Y. Wang, and H. F. Chau, Fully Passive Quantum Conference Key Agreement, arXiv:2407.15761.
- [79] C. Q. Hu, W. Y. Wang, K. S. Chan, Z. H. Yuan, and H. K. Lo, Proof-of-Principle Demonstration of Fully Passive Quantum Key Distribution, *Phys. Rev. Lett.* **131**, 110801 (2023).
- [80] F. Y. Lu, Z. H. Wang, V. Zapatero, J. L. Chen, S. Wang, Z. Q. Yin, M. Curty, D. Y. He, R. Wang, W. Chen, G. J. Fan-Yuan, G. C. Guo, and Z. F. Han, Experimental demonstration of fully passive quantum key distribution, *Phys. Rev. Lett.* **131**, 110802 (2023).